Article

Petrographic Evaluation of Aggregate from Igneous Rocks: Alkali–Silica Reaction Potential

Aneta Antolik *[ID], Mariusz Dąbrowski [ID] and Daria Jóźwiak-Niedźwiedzka [ID]

Institute of Fundamental Technological Research, Polish Academy of Sciences, A. Pawińskiego 5b, 02-106 Warsaw, Poland; mdabrow@ippt.pan.pl (M.D.); djozwiak@ippt.pan.pl (D.J.-N.)
* Correspondence: aantolik@ippt.pan.pl; Tel.: +48-826-12-81 (ext. 207)

Abstract: A thorough petrographic evaluation of aggregates from igneous rocks in terms of their alkali–silica reaction (ASR) potential is crucial in ensuring the durability and long-term performance of concrete structures, especially those where access to additional alkalis is possible, such as from de-icing agents. The aim of the research was to assess the potential reactivity of aggregates from igneous rocks, as only such aggregates are used for concrete airport pavements in Poland. Petrographic analysis was conducted to identify the reactive minerals in the aggregate, and it was extended by quantitative image analysis. The strained, microcrystalline and cryptocrystalline quartz were found to be reactive components but significantly differed in content. It was found that aggregates from igneous rocks were characterized by different susceptibility to ASR and that methods to mitigate the occurrence of ASR should be considered to be used in airfield concrete. A relationship between the content of analyzed reactive minerals and the expansion of mortar bars in AMBT, as well as of the concrete prism in the CPT method, was revealed.

Keywords: igneous rocks; granite aggregate; mineral composition; thin sections; digital image analysis; petrographic analysis; alkali–silica reaction; concrete durability

1. Introduction

Airfield pavements are designed to support the weight of aircraft, withstand heavy loads and traffic distribution, and resist damage from the environment and other external factors. Concrete is commonly used for airfield pavements because of its mechanical characteristics, durability, and resistance to damage from chemicals and oil spills. This type of concrete facility is an essential component of airport infrastructure, and its proper design, construction and maintenance are critical to ensuring the safety and efficiency of air travel [1,2]. However, concrete pavements are particularly exposed to alkali–silica reactions (ASR) due to the penetration of alkalis from de-icing agents [3–5]. Rangaraju et al. [3] showed that acetates used for de-icing airports cause significant destruction due to ASR. Giebson et al. [4] proposed the possible mechanism of influence of de-icers on ASR as an excess supply of alkalis and the release of OH^- ions due to the increased solubility of $Ca(OH)_2$. Glinicki et al. [5] presented that concrete pavement with reactive aggregate, exposed to sodium chloride, was destroyed due to ASR. Alkali–silica reaction is caused by the reaction between alkalis (sodium and potassium hydroxide) in the concrete pore solution and certain types of reactive silica constituents present in some aggregates [6]. The ASR produces a gel-like substance that can absorb water and expand over time, leading to cracking and other types of damage in the concrete. Despite the developed standard methods concerning the potential of aggregate to provoke alkali–silica reaction, and concrete itself, and the methods of mitigating this harmful reaction, ASR remains one of the main problems of the durability of concrete structures [7].

Selecting appropriate concrete components, such as aggregate that does not contain reactive minerals, is one of the easiest methods to avoid the alkali–silica reaction in concrete.

As suggested by Poole [8], the constituents of the rock, rather than the type of rock, should be taken into account as the criteria for the ASR potential of the aggregate. The vast majority of aggregates intended for concrete contain quartz, but its reactivity varies. Studying the relationship between deformation processes and the microstructural characteristics of rocks can provide valuable insights into the behavior of quartz-bearing aggregates in concrete [9]. Amorphous SiO_2 (e.g., opal) is recognized as one of the most highly reactive form of quartz, followed by meta-stable crystals like cristobalite and tridymite, microcrystalline silica, and other crystalline structures with abundant lattice defects, residual strain, or internal microcracks [6,10]. Locati et al. [9] revealed that the reactivity of quartz-bearing mylonites increased by ~30% compared to the non-mylonitized specimen due to the increment in the strained quartz content. Bourdot et al. [11] found that the grain size of SiO_2 was a supplementary key parameter, in addition to crystallinity and strain, since it could promote ASR development with siliceous aggregates. In a recent study, Custódio et al. [12] found that almost all aggregates used in recently constructed Portuguese dams contain potentially alkali–silica reactive forms of SiO_2 (e.g., mainly quartz precipitates in feldspars, deformed and microcrystalline quartz grains). In addition, it was shown that the aggregates also contained minerals that can release alkalis into the concrete pore solution (e.g., feldspar or muscovite).

The degree of occurrence or rate of ASR depends mainly on the type of constituent materials used, i.e., aggregate and cement. The composition of concrete used for airfield pavements, described in detail in Polish technical standard NO-17-A204:2015 [13], requires the use of granite aggregate. For airport pavement concrete, granite with a maximum grain size of 31.5 mm and homogeneous petrographic composition is required as the coarse aggregate. However, it is not allowed to use blended cement for airport pavements, which could reduce the potential alkali reactivity of the aggregate in concrete [14,15]. Therefore, the initial assessment of this aggregate takes on special importance.

Aggregates made from igneous rocks, especially granites, are generally regarded as harmless or improbable to exhibit reactivity to alkalis in concrete [16,17] due to the possible presence of small amounts of microcrystalline or undulatory or subgrained crystalline quartz [18]. Jóźwiak-Niedźwiedzka et al. [17] tested the reactivity of different aggregates from igneous rocks and showed that gabbro and granite were considered to be nonreactive. Ramos et al. [16] concluded that granite aggregates require an extension of the standard research methods, due to their delayed reactivity. Nevertheless, the literature reports indicate the occurrence of various damages in large-scale constructions produced with granitic aggregates as a result of ASR [19–21]. Hence, it is essential to consider granite as nonreactive in specific regions, while acknowledging that certain varieties of granite in different areas exhibit reactivity [18]. Explicit determination of rocks' reactivity based on their geological term is impossible. The reactivity of aggregates from igneous rocks can vary, depending on the specific mineralogy and composition of the deposit. Some aggregates may contain higher levels of reactive minerals or may be more susceptible to alteration due to weathering or other environmental factors [22], which can increase the potential for ASR. In previous studies, the authors [23] primarily examined the effect of strained quartz on the occurrence of the alkali–silica reaction in granite aggregates, which were considered nonreactive. However, the simultaneous impact of microcrystalline quartz, cryptocrystalline quartz, and strained quartz, as well as aggregates from igneous rocks other than granites, on alkali–silica reactivity has not been taken into consideration.

Reactive silica quantification is a critical step in evaluating the potential for ASR in aggregates. Image analysis techniques can be helpful in accurately determining the content and distribution of reactive silica minerals, while advanced research techniques based on image analysis mainly concern the estimation of the volume ratio of finer aggregates [24], the analysis of the impact of aggregate segregation on concrete mechanical parameters [25], investigation of the changes of aggregate shape, i.e., form, angularity, and texture during different aggregate abrasion/degradation tests [26], or the degree and size of cracking of the cement matrix and aggregate [27,28]. The establishment of a robust methodology

for petrographic characterization of aggregates using image analysis, and evaluation of the effectiveness of this approach in identifying and quantifying reactive silica minerals associated with ASR, are not so common. Bourdot et al. [29] identified the potentially reactive silica forms in tested aggregates; however, it was a qualitative approximation. Castro and Wigum [30] revealed that image analysis has proven to be a precise and accurate method for grain size and grain shape analysis of aggregates for concrete, but no correlation was found between the average values of the grain-shape descriptors and the laboratory tests to assess the potential reactivity of the aggregates.

This study presents the contribution of petrography and digital image analysis in expanding the knowledge of the alkali–silica reaction applied to domestic aggregate from igneous rocks including granite, granodiorite and gabbro. The study primarily concentrated on the microscopic examination of reactive minerals present in igneous-origin aggregates through thin sections and quantitative analysis. The specific image analysis algorithms to identify and quantify the amount of reactive silica minerals in the analyzed aggregate were proposed. The outcomes of the petrographic analysis were compared to the expansion findings of the alkali–silica reactivity.

2. Materials and Methods

2.1. Materials

The subject of the research was aggregates from the six largest quarries of igneous rocks in Poland, located in the Sudeten Mountains: 3 granite aggregates (G1, G2, G3), 1 granodiorite aggregate (GD) and 2 gabbro aggregates (GA1, GA2). The granite aggregates were characterized by similar densities, of 2.63 ± 0.03 g/cm^3, and chemical compositions, Table 1. The largest differences were found in the content of SiO_2 ($73.9 \pm 1.5\%$), Al_2O_3 ($14.0 \pm 0.7\%$), K_2O ($4.2 \pm 0.5\%$), CaO ($1.4 \pm 0.3\%$) and Na_2O ($3.7 \pm 0.3\%$). The granodiorite aggregate was characterized by a density of 2.69 g/cm^3 and the gabbro aggregates by 2.91 ± 0.05 g/cm^3. The chemical composition of the granodiorite and gabbro aggregates differed from the granite aggregates. They contained a smaller amount of silica and a larger amount of iron oxide, magnesium oxide and calcium oxide in comparison to the granite aggregates.

Table 1. XRF chemical composition of aggregates from igneous rocks, % wt.

Compound	SiO_2	TiO_2	Al_2O_3	Fe_2O_3	MnO	MgO	CaO	Na_2O	K_2O	P_2O_5	(SO$_3$)	(Cl)	(F)
G1 [%]	75.77	0.13	13.03	1.16	0.03	0.15	1.15	3.35	4.48	0.04	<0.01	0.02	<0.01
G2 [%]	74.14	0.12	14.00	1.26	0.03	0.19	0.86	3.54	5.06	0.12	<0.01	0.02	<0.01
G3 [%]	71.60	0.22	15.01	1.47	0.04	0.34	1.38	4.16	3.78	0.07	<0.01	<0.001	<0.10
GD [%]	56.87	0.89	13.65	7.86	0.14	5.72	6.76	2.5	3.58	0.96	0.10	0.04	<0.01
GA1 [%]	46.59	0.86	13.49	10.44	0.16	10.81	10.89	2.44	0.15	0.14	<0.01	0.013	<0.01
GA2 [%]	45.83	0.88	13.92	11.06	0.15	11.34	11.26	2.31	0.23	0.08	<0.01	0.02	<0.01

Ordinary Portland cement, CEM I 52.5 R, with $Na_2O_{eq} = 0.87\%$ was used in the research. The detailed chemical composition of the cement is presented in [23].

2.2. Methods

2.2.1. Characteristics of the Aggregates

The chemical composition of the aggregates was determined on powdered specimens by Wavelength Dispersive X-ray Fluorescence Spectrometer (WDXRF), Philips PW 2400 (Amsterdam, The Netherland).

Volume density was determined according to the PN-EN-1097–6:2002 standard [31].

The mineral composition of the aggregates was analyzed using thin sections (25 × 40 mm). For each analyzed aggregate, four thin sections were prepared. Before embedding in epoxy

resin with a fluorescent dye, the aggregate was crushed to a 2–4 mm fraction, and then washed and dried at 100 °C for 24 h. After the resin had hardened, the specimens were ground and polished. The grinding and initial polishing were carried out on silicon carbide abrasive papers with a grit size of P 100–P 1200, mounted on the rotating grinder-polisher Presi Mecatech 334 (France). The final polishing was performed using diamond pastes with a grit size of 9, 6, 3, 1 and 0.25 μm on polishing cloths. The prepared specimen was attached to a microscope slide, and excess material was removed using a diamond saw. The grinding and polishing process was repeated on the other side of the specimen and continued in the same sequence until the desired thickness of 30 ± 2 μm was achieved. The thickness of the specimen was standardized to ensure unambiguous mineral recognition (using the quartz's reference color).

Petrographic observations were made using an Olympus BX51 (Tokyo, Japan) polarizing microscope and an automatic stage Prior ES11BX/B (United Kingdom). The thin sections were analyzed in polarized light—both crossed (XPL) and plain (PPL)—as well as crossed with gypsum plate (G-XPL).

2.2.2. Digital Image Analysis

A quantitative analysis of minerals identified in the petrographic microscope was performed according to the proposed method. Observations were carried out in two options: XPL and GXPL (separately). Single images with dimensions of 2.2×1.65 mm and high resolution (1 px = 0.86 μm) were collected from the entire surface of the thin sections and then combined into one image using Image Composite Editor software. The analysis of the obtained images was carried out using Image Pro Plus software. At the start, the separation of the aggregate grains from the background (resin) was performed. For this purpose, images made in the presence of a gypsum plate were used. The use of a fluorescent dye made the background orange in the crossed polarized light with the gypsum plate, which greatly facilitated the separation of aggregate grains. The main minerals of intrusive igneous rocks were analyzed: quartz, feldspar, olivine and biotite. Due to the simplification of the analysis, minerals that were in small amounts were classified into one category: other (e.g., muscovite, hornblende, amphibole, pyroxene). The analysis was focused on the reactive minerals; therefore, the quartz was further divided into nonreactive and reactive (strained, microcrystalline and cryptocrystalline). Based on the long-term experience of the operator, the components were manually marked, and the selection of reactive components was performed. The microcrystalline (10–100 μm) and cryptocrystalline (<10 μm) quartz were distinguished by grain size. According to the literature data [32], strained quartz with an angle of undulatory extinction above 15° is reactive, while other sources report an angle of 25° [33]. To simplify the analysis and reduce the experimenter's error, the angle of undulatory extinction was not considered in each aggregate grain, but only in a few doubtful cases. Due to the fact that the image of the entire thin section was subjected to digital analysis after the assembly operation, checking the extinction angle each time on the microscope was troublesome and time-consuming. To determine the angle of undulatory extinction in these few cases, a microscope with a rotating stage was used. The strained quartz was classified as reactive (highly strained) if the undulatory extinction angle was greater than 15° [32]; if less, it was considered nonreactive (low-strained). However, this did not have a major impact on the result, due to the predominant number of grains with highly strained quartz, in which it was not necessary to check the angle. Based on these manual markings, the components were automatically separated using the Image Pro Plus software, and their total percentage surface area relative to the surface area of the aggregate grains was calculated. The method that was proposed has some limitations, including the dependence on the experimenter's experience. However, such a limitation is known and taken into account in studies on the petrographic analysis of aggregate. For example, the ASTM C 295 [34] standard describes the required qualifications of people performing petrographic research and recommends that the test should be carried out

by a petrographer with at least 5 years of experience in petrography in testing concrete materials.

Figure 1 shows an image of a thin section (granite aggregate G3) in which individual minerals are distinguished.
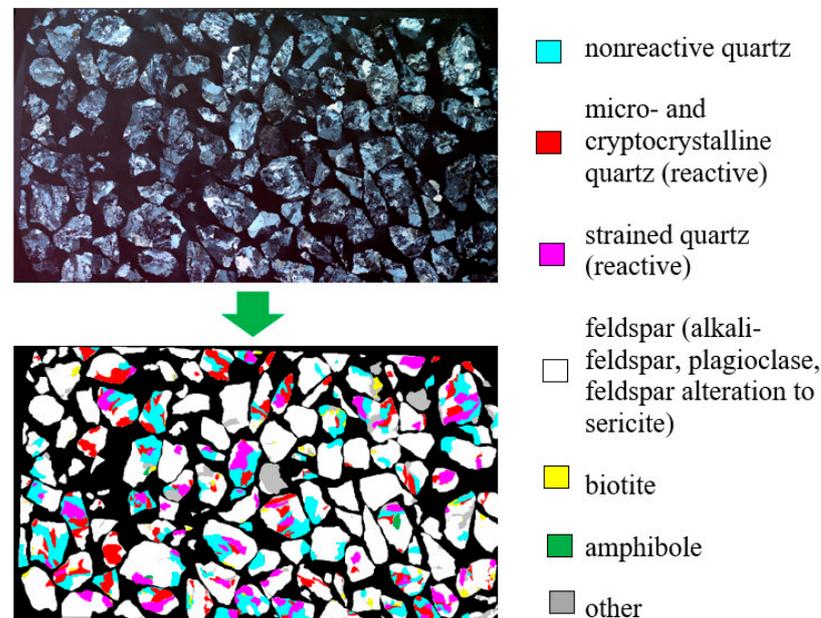
Figure 1. Digital image analysis of thin section (aggregate G3) applied to quantitative analysis of minerals: nonreactive quartz, micro- and cryptocrystalline quartz, strained quartz, feldspar (including alkali–feldspar, plagioclase, feldspar alteration to sericite), biotite, other (muscovite, hornblende); image size 25 × 40 mm.

2.2.3. Alkali–Silica Reactivity

In order to compare the alkali–silica reactivity and validate the results from the digital image analysis, standard tests according to ASTM C1260 [35] and ASTM C1293 [36] were performed. The first method, which is called the accelerated mortar bar test (AMBT), consists of expansion measurements of mortar specimens that are exposed to 80 °C and 1 M NaOH for 14 days (28 days for airport pavement). According to this method, the aggregate is considered to be potentially reactive if expansion after 14 days is above 0.10%. The second method (concrete prism test, CPT) involves expansion measurements of concrete specimens that are exposed to 38 °C and high humidity for 365 days. According to this method, the expansion limit for potentially reactive aggregate is above 0.04% after 365 days.

2.2.4. Scanning Electron Microscopy Analysis

A scanning electron microscope (SEM) with energy-dispersive X-ray spectroscopy (EDS) was used for the observations of specimens cut from mortar bars after the ASTM C1260 test. The JEOL JSM-6460LV microscope with an EDS detector was used. Polished specimens were analyzed. The observations were focused on alkali–silica reaction products. The observations were carried out using an acceleration voltage of 20 kV and a working distance of 10 mm in the backscattered electron mode. The polished specimens were additionally sputtered with carbon to make the samples conductive and avoid charging effects, which increased the resolution.

3. Results

Petrographic analysis was carried out on the thin sections in transmitted light. The examples illustrating the analyzed aggregates from the igneous rocks are shown in Figure 2 (in XPL) and Figure 3 (in PPL).
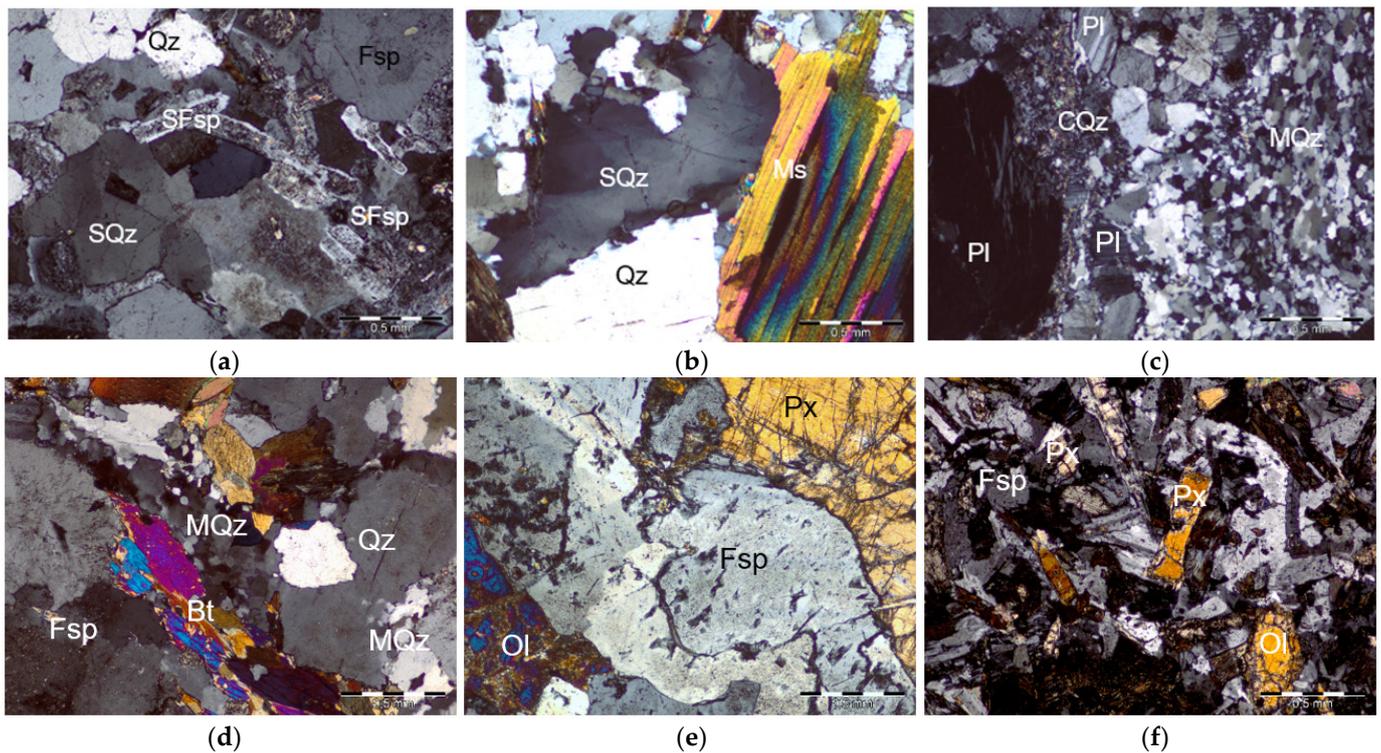
Figure 2. Petrographic images of aggregates from igneous rocks in cross-polarized light: (**a**) G1, (**b**) G2, (**c**) G3, (**d**) GD, (**e**) GA1, (**f**) GA2. Minerals: Qz—nonreactive quartz, SQz—strained quartz, MQz—microcrystalline quartz, CQz—cryptocrystalline quartz, Ms—muscovite, Ol—olivine, Fsp—feldspar, SFsp—feldspar alteration to sericite, Bt—biotite, Hb—hornblende, Px—pyroxene; scale bar = 0.5 mm.

The analyzed granite aggregates were characterized by a similar mineralogical composition. Quartz and feldspar (including alkali-feldspar and plagioclase) were found as the main components. Also, biotite and amphibole were identified. Conversion to sericite was identified in the feldspar and the highest content of biotite in the G1 granite aggregate. According to quantitative analysis, feldspar constituted the largest part of the granite aggregates, from 52.2% to 63.4%. Due to the simplification of the image analysis, this group included both alkali–feldspar, plagioclase and feldspar alteration to sericite. Quartz in the granite aggregates was from 29.3% to 38.1%. Granodiorite aggregate, GD, was characterized by a smaller amount of quartz (20.2%) and higher content of biotite (15.3%) in comparison to granite aggregate. Both gabbro aggregates, GA1 and GA2, had similar mineral compositions. The gabbro aggregates were characterized by a smaller content of quartz (<5%) in comparison to the granite aggregates. The GA1 and GA2 contained significant amounts of pyroxene (>20%) and olivine (GA1: 12.4%, GA2: 5.1%). All the aggregates from igneous rocks were analyzed for the presence of reactive minerals, due to the potential of an alkali–silica reaction. Microcrystalline (10–100 μm) and cryptocrystalline (<10 μm) quartz were found in trace amounts (max. 0.2%) in granites, G1 and G2, and granodiorite, GD, while strained quartz was present in greater quantities (2.0; 4.7 and 2.7%, respectively). However, the G3 granite aggregate contained much higher amounts of microcrystalline, cryptocrystalline and strained quartz (6.1 and 7.4%, respectively). Both gabbro aggregates contained trace amounts of reactive forms of quartz (max. 0.2%). A detailed quantitative analysis of the minerals, especially reactive, is presented in Table 2.
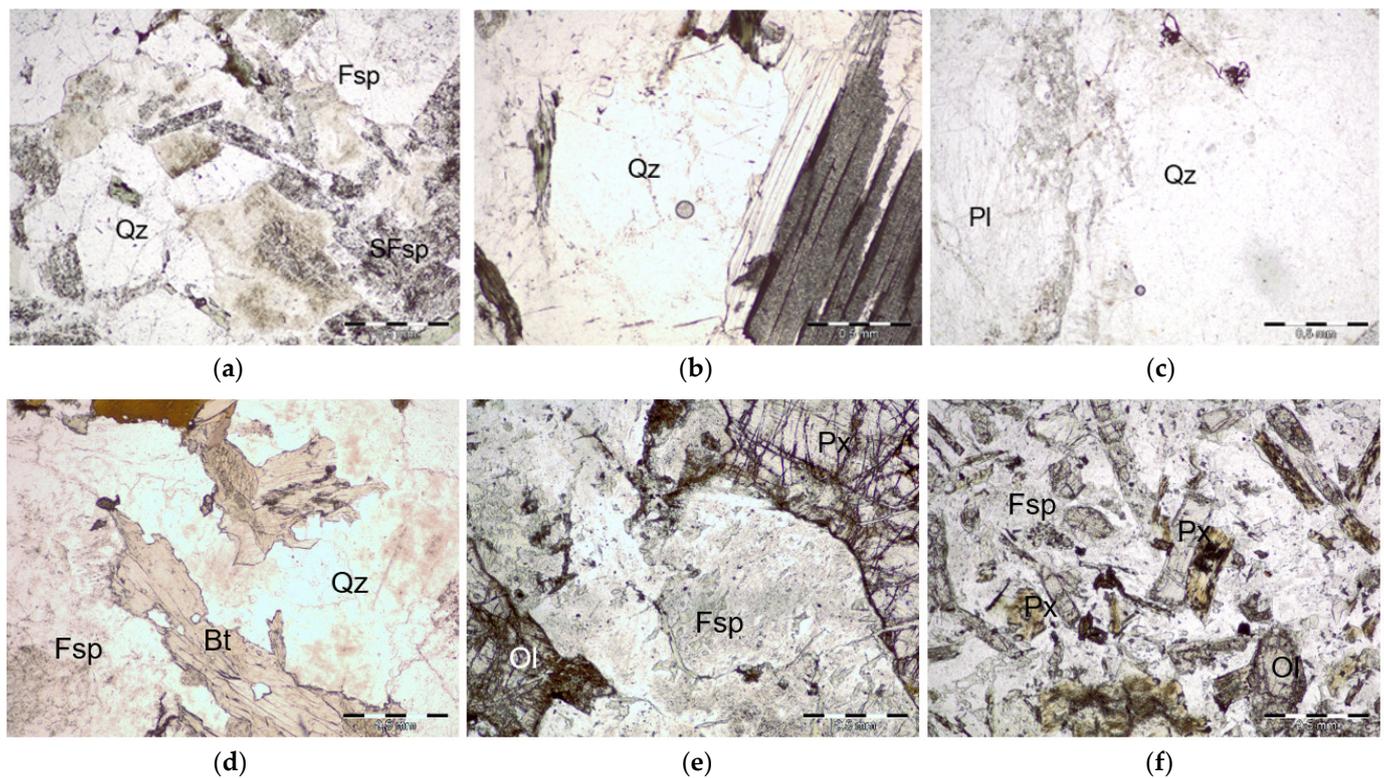
Figure 3. Petrographic images of aggregates from igneous rocks in plain polarized light: (**a**) G1, (**b**) G2, (**c**) G3, (**d**) GD, (**e**) GA1, (**f**) GA2. Minerals: Qz—quartz, Ol—olivine, Fsp—feldspar, SFsp—feldspar alteration to sericite, Bt—biotite, Hb—hornblende, Px—pyroxene; scale bar = 0.5 mm.

Table 2. The results of the quantitative analysis of the mineral composition of aggregates from igneous rocks based on digital image analysis.

Aggregate	Quartz			Feldspar	Biotite	Amphibole	Pyroxene	Olivine	Other
	Strained (Reactive)	Micro- and Cryptocrystalline (Reactive)	Other Forms (Nonreactive)						
G1 [%]	2.0 ± 0.1	0.1 ± 0.1	36.0 ± 1.4	52.2 ± 1.7	5.4 ± 0.3	2.4 ± 0.2	0	0	1.9 ± 0.2
G2 [%]	4.7 ± 0.2	0.2 ± 0.1	29.1 ± 1.1	57.3 ± 1.8	2.6 ± 0.1	2.1 ± 0.2	0	0	4 ± 0.3
G3 [%]	7.4 ± 0.3	6.1 ± 0.3	15.8 ± 0.5	63.4 ± 2.5	2.1 ± 0.1	1.7 ± 0.2	0	0	3.5 ± 0.2
GD [%]	2.7 ± 0.2	0.2 ± 0.1	17.3 ± 0.5	57.4 ± 1.5	15.3 ± 0.6	4.1 ± 0.3	1.6 ± 0.2	0	1.4 ± 0.2
GA1 [%]	0.2 ± 0.1	0.1 ± 0.1	3.7 ± 0.3	59.3 ± 2.1	0.7 ± 0.1	1.2 ± 0.2	21.3 ± 1.1	12.4 ± 0.5	1.1 ± 0.2
GA2 [%]	0.1 ± 0.1	0.1 ± 0.1	4.2 ± 0.4	60.1 ± 2.2	0.5 ± 0.1	1.5 ± 0.2	25.2 ± 1.7	5.1 ± 0.4	3.0 ± 0.3

Results of the expansion of mortar bars (AMBT) are presented in Figure 4. Only one granite aggregate (G3) showed an expansion of over 0.1% after 14 days of exposure to 1 M NaOH at 80 °C. However, extending the test to 28 days did not stop the expansion, which proceeded at a similar rate. Three of the six aggregates (G2, G3, GD) showed an expansion greater than 0.1% after 28 days. The results of the expansion of the concrete prisms (CPT) are presented in Table 3. In the long-term test, concrete expansion above the allowable limit of 0.04% was found for two aggregates (G2, G3). These aggregates were also characterized by the highest content of strained quartz, microcrystalline quartz and cryptocrystalline quartz.
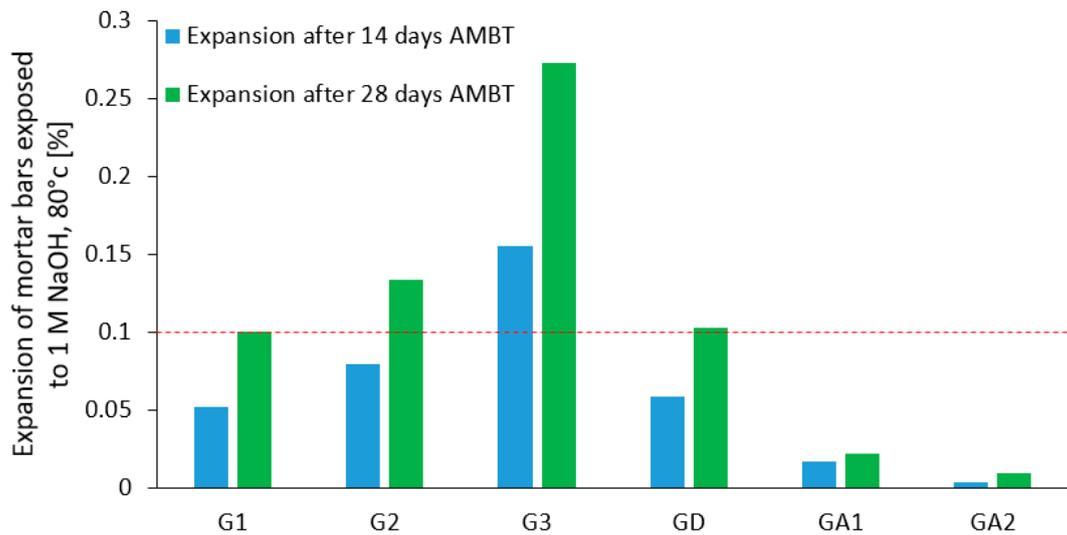
Figure 4. Results of expansion of mortar bars (AMBT) after 14 and 28 days.

Table 3. Results of the expansion of concrete prisms (CPT) after 365 days.

Concrete with Aggregate	G1	G2	G3	GD	GA1	GA2
Expansion after 365 days CPT [%]	0.030	0.047	0.056	0.034	0.023	0.014

After the AMBT and CPT tests, the specimens were subjected to microscopic examination to identify alkali–silica reaction products. In the mortar bars and concrete prisms with granite and granodiorite aggregates, signs of ASR were found. The aggregate grains as well as the cement matrix were cracked. The majority of the ASR gel was detected specifically within cracks found within the aggregate particles. The presence of air voids filled with ASR products was also confirmed. ASR gel was identified as amorphous rather than crystalline. Examples of the ASR gel are presented in Figures 5–8. In the specimens with gabbro aggregates, the presence of ASR signs was not confirmed. The ASR gel chemical composition was typical, and it did not depend on the type of aggregate (granite or granodiorite): $(Na+K)/Si\sim0.20$–0.30 $Ca/Si\sim0.30$–0.40.
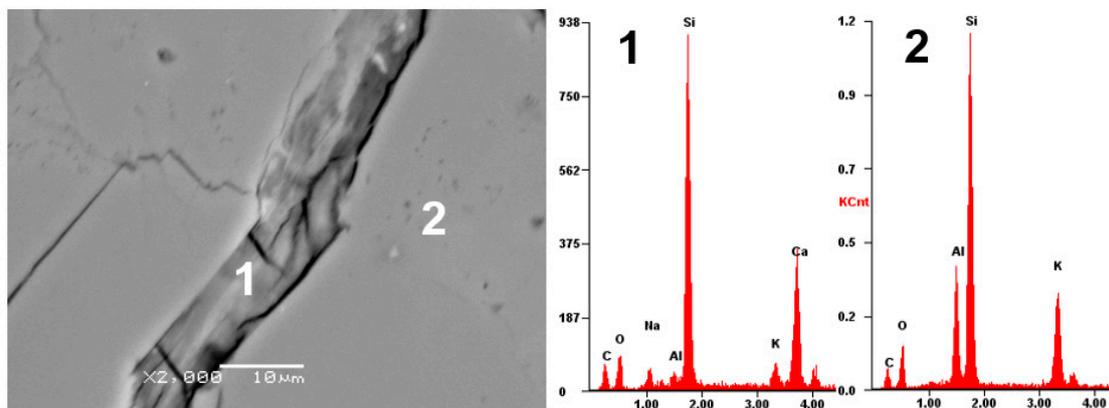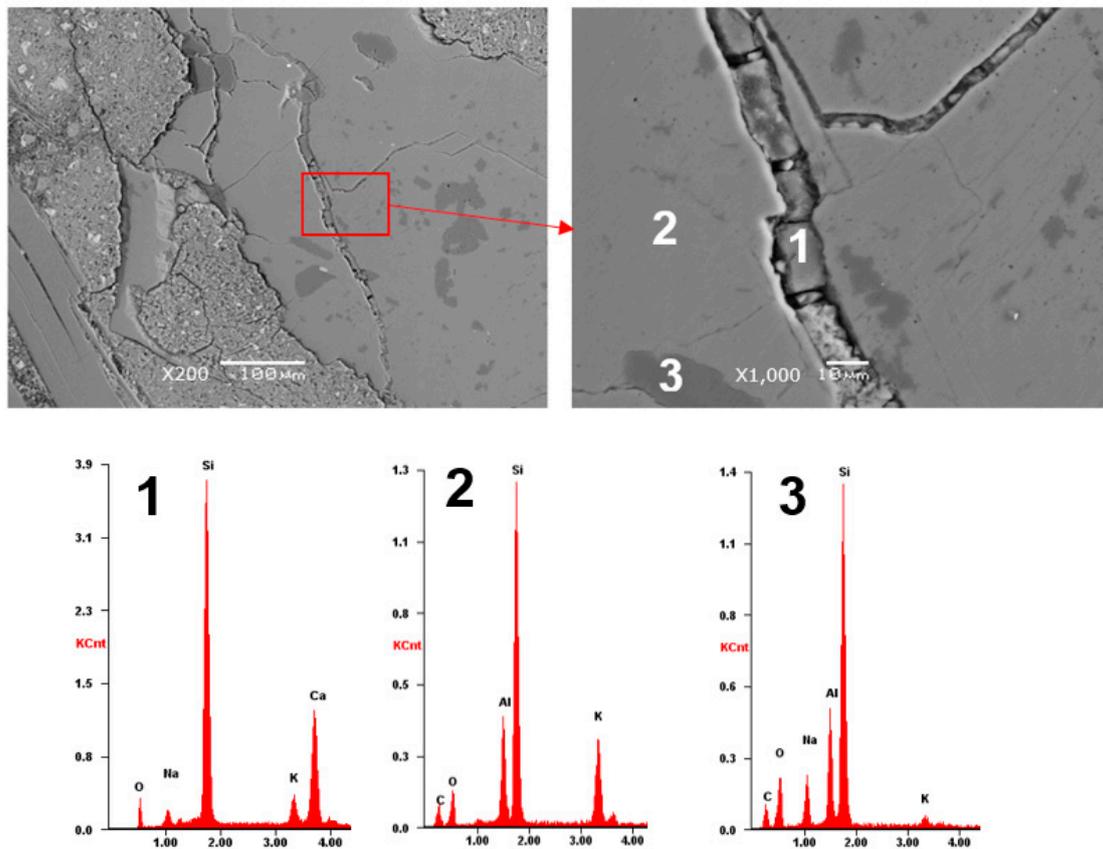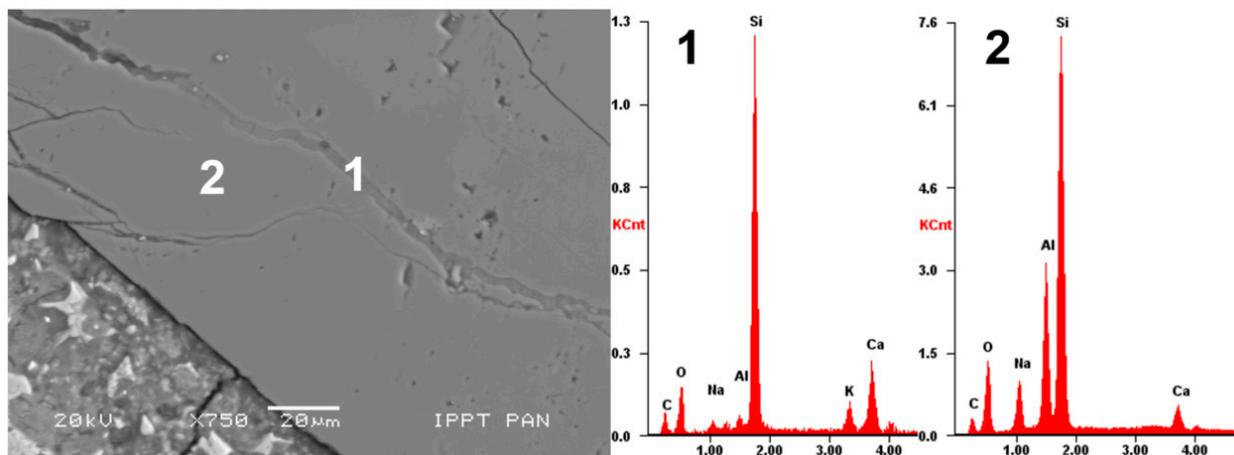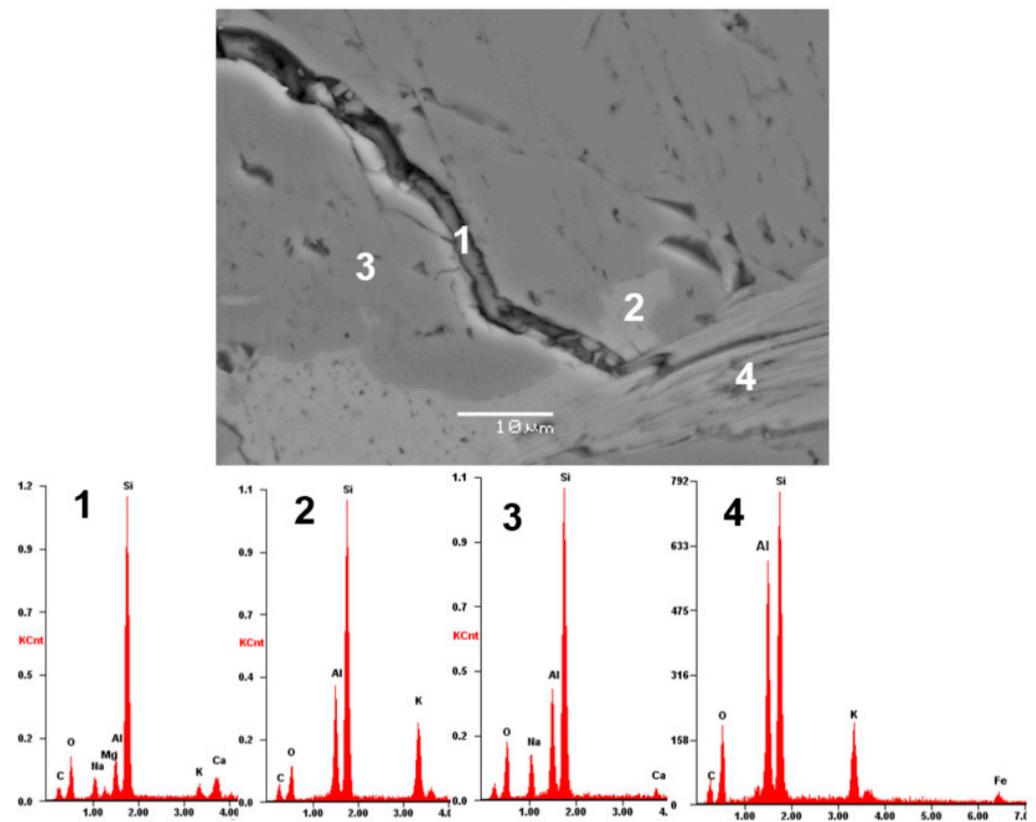

Figure 5. Crack in granite aggregate (G3) grain filled with ASR gel, with analysis of chemical composition (EDS): (1) Si-Ca-K-Na gel, (2) potassium feldspar; after AMBT test.

Figure 6. Cracks in granite aggregate (G2) grain filled with ASR gel, with analysis of chemical composition (EDS): (1) ASR gel, (2) potassium feldspar, (3) sodium feldspar; after AMBT test.

Figure 7. Cracks in granite aggregate (G1) grain filled with ASR gel, with analysis of chemical composition (EDS): (1) ASR gel, (2) sodium feldspar; after CPT test.

Figure 8. Crack in granodiorite aggregate (GD) grain filled with ASR gel, with analysis of chemical composition (EDS): (1) ASR gel with traces of Al, (2) potassium feldspar, (3) sodium feldspar, (4) muscovite; after CPT test.

The petrographic results obtained on the thin sections were confirmed by the results of the expansion of mortar bars and concrete prisms. The rate of expansion confirmed the petrographic observations, in which reactive minerals like strained, microcrystalline and cryptocrystalline quartz were identified. In addition, the detailed observations of the microstructure after testing according to ASTM C1260 and ASTM C1293 confirmed the presence of ASR reaction products in the specimens with granite and granodiorite aggregates.

4. Discussion

Previous studies concerning granite aggregates have been conducted assigning this type of aggregate to the group of nonreactive or slowly reacting aggregates [16,18]. In [37], the authors made an attempt to determine the amount of reactive form of quartz, taking into account the crystal grain size, which is detrimental to further concrete durability due to ASR. By comparing these findings to the expansion observed after AMBT, they established a correlation and achieved alignment, particularly when considering various forms of quartz simultaneously. They stated that microcrystalline quartz was the most harmful mineral component, and strained quartz showed less susceptibility to ASR. The quantitative differentiation of the reactive minerals in the aggregate allows for a more accurate determination of their reactivity potential. In studies conducted on domestic aggregates from igneous rocks (granite, granodiorite and gabbro), strained, microcrystalline and cryptocrystalline quartz were used for analysis. However, on the basis of the obtained quantitative results of the content of reactive minerals, and the results of mortar and concrete expansion, it cannot be unequivocally confirmed that microcrystalline and cryptocrystalline quartz have much higher reactivity compared to strained quartz. The very high expansion of the mortar and concrete with the G3 aggregate was the result of the total high content of reactive minerals,

microcrystalline, cryptocrystalline and strained quartz. Other aggregate components, such as feldspar or biotite, which may be a source of additional alkalis in concrete, probably had a marginal role in accelerating ASR.

The quantitative petrographic analysis of reactive mineral content in the aggregates from igneous rocks and the evaluation of alkali–silica reactivity using the ASTM C1260 method led to the establishment of a relationship between them in the form of power function $y = f(x^{1/2})$ ($R^2 = 0.99$). The results of the petrographic analysis correlate with the results of alkali–silica reactivity (Figure 9). Observing a positive correlation, increased expansion was noted as the content of strained, microcrystalline, and cryptocrystalline quartz in the aggregate grew. An examination has already been conducted on the impact of strained quartz content in granite aggregates by the authors [23]; however, the scope of the aggregates tested was limited to granite rocks.
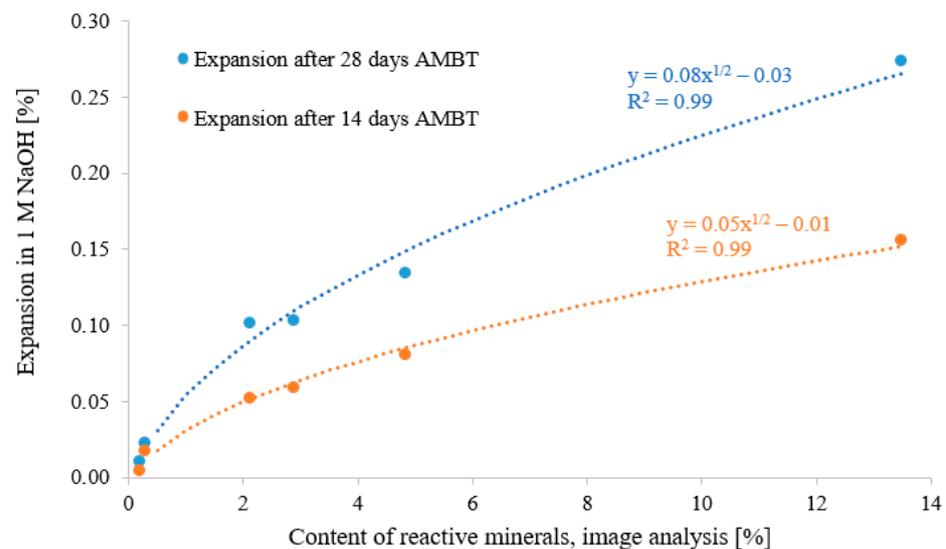
Figure 9. Expansion of mortar specimens after testing according to ASTM C1260 for 14 and 28 days versus content of reactive minerals (digital image analysis).

It turns out that expanding the base of aggregates from igneous rocks and summing up all reactive minerals allows for a very high adjustment to the expansion dependence on the content of reactive minerals. A similar correlation was obtained for Malaysian granites [38] but for higher volumes of reactive forms of quartz (3%–33%). However, the relationship was the exponential function and was not so statistically significant ($R^2 = 0.72$) as in the conducted research. The expansion increased with the increase in total strained and microcrystalline quartz content, while the results obtained by Ramos et al. [39] performed on the granitic specimens led to the conclusion that the ASTM C1260 mortar bar test demonstrated a weak association with the petrographic characterization of the aggregate.

The correlation of concrete prism expansion after 1 year of testing according to ASTM C1293 with the content of reactive minerals was also at a good level (Figure 9). There is visible a general tendency in the form of power function $y = f(x^{1/2})$, $R^2 = 0.93$ (Figure 10). The difference in the results of the accelerated and long-term methods may be related to the prolonged incubation time for slow-reacting aggregates tested according to ASTM C1293 [40] or alkali leaching [41]. Preliminary test results for alkali leaching during the ASTM C1293 test are currently under investigation.
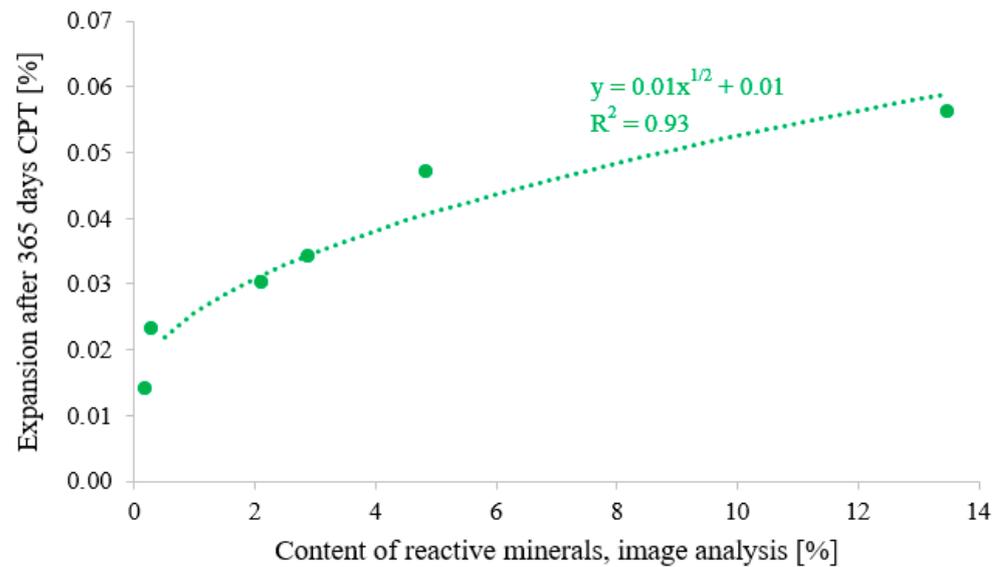
Figure 10. Expansion of concrete specimens after testing according to ASTM C1293 for 365 days versus content of reactive minerals (digital image analysis).

The use of digital image analysis for quantitative analysis to assess reactive minerals in aggregates from igneous rocks aligns well with the expansion observed in the accelerated mortar bar test. It has been shown that the applied quantitative image analysis can be successfully used to identify and quantify reactive minerals in aggregates with greater precision than traditional petrographic analysis.

While aggregates from igneous rocks are generally considered to be a low-risk aggregate for ASR, it is still important to perform tests and analysis to ensure that the specific type of aggregates, especially granites, being used in concrete airfield pavements do not pose a significant risk for ASR, particularly in environments where additional alkali from de-icing agents are expected. The mineral composition of aggregates from igneous rocks can vary widely depending on their source, and some types of aggregates may contain reactive silica minerals that could potentially lead to ASR in concrete.

5. Conclusions

From the conducted tests, the following can be concluded:

- The study, which was based on microscopic characterization, found that feldspars were the main components present in all aggregates from the igneous rocks that were analyzed.
- Strained, microcrystalline and cryptocrystalline quartz were found in significant amounts in granite and granodiorite aggregates. In gabbro aggregates, reactive minerals were present in trace amounts.
- The granite aggregates contained from 2.0 to 7.4% of strained quartz and from 0.1 to 6.1% of microcrystalline and cryptocrystalline quartz. The granodiorite aggregate contained 2.7% of strained quartz and 0.2% of microcrystalline and cryptocrystalline quartz; however, the gabbro aggregate contained only up to 0.2% of strained, microcrystalline and cryptocrystalline quartz.
- According to the standard ASTM tests, one granite aggregate (G3) was found reactive, according to AMBT (after 14 days), and two aggregates (G2, G3) according to CPT.
- The most reactive granite, G3, aggregate contained the highest amount of reactive minerals, especially microcrystalline and cryptocrystalline quartz.
- The microscopic analysis confirmed the presence of ASR products in the specimens after AMBT and CPT, but only with the granite and granodiorite aggregates. In the specimens with the gabbro aggregates, ASR products were not found.

- A power function, y = f(x$^{1/2}$), between the content of reactive minerals and expansion after 14 and 28 days of mortar bars in AMBT was found, as well as 365 days of concrete prism in CPT.

References

1. Shen, Z.; Liu, B.; Zhou, G. Stressing State Analysis of Concrete Airport Pavement by Modeling Experimental Strain Data. *Case Stud. Constr. Mater.* **2022**, *17*, e01635. [CrossRef]
2. Zhou, C.; Lan, G.; Cao, P.; Tang, C.; Cao, Q.; Xu, Y.; Feng, D. Impact of Freeze-Thaw Environment on Concrete Materials in Two-Lift Concrete Pavement. *Constr. Build. Mater.* **2020**, *262*, 120070. [CrossRef]
3. Rangaraju, P.R.; Sompura, K.R.; Olek, J. Investigation into Potential of Alkali-Acetate-Based Deicers to Cause Alkali-Silica Reaction in Concrete. *Transp. Res. Rec.* **2006**, *1979*, 69–78. [CrossRef]
4. Giebson, C.; Seyfarth, K.; Stark, J. Influence of Acetate and Formate-Based Deicers on ASR in Airfield Concrete Pavements. *Cem. Concr. Res.* **2010**, *40*, 537–545. [CrossRef]
5. Glinicki, M.A.; Jóźwiak-Niedźwiedzka, D.; Antolik, A.; Dziedzic, K.; Dąbrowski, M.; Bogusz, K. Diagnosis of ASR Damage in Highway Pavement after 15 Years of Service in Wet-Freeze Climate Region. *Case Stud. Constr. Mater.* **2022**, *17*, e01226. [CrossRef]
6. Rajabipour, F.; Giannini, E.; Dunant, C.; Ideker, J.H.; Thomas, M.D.A. Alkali–Silica Reaction: Current Understanding of the Reaction Mechanisms and the Knowledge Gaps. *Cem. Concr. Res.* **2015**, *76*, 130–146. [CrossRef]
7. Nixon, P.J.; Sims, I. RILEM Recommendations for the Prevention of Damage by Alkali- Aggregate Reactions in New Concrete Structures. In *State-of-the-Art Report of the RILEM Technical Committee219-ACS*; Springer: Berlin/Heidelberg, Germany, 2016; ISBN 9789401772518.
8. Poole, A.B. Introduction to Alkali-Aggregate Reaction in Concrete. In *The Alkali-Silica Reaction in Concrete*; CRC Press: London, UK, 1992.
9. Locati, F.; Marfil, S.; Baldo, E. Effect of Ductile Deformation of Quartz-Bearing Rocks on the Alkali-Silica Reaction. *Eng. Geol.* **2010**, *116*, 117–128. [CrossRef]
10. Jóźwiak-Niedźwiedzka, D.; Gibas, K.; Glinicki, M.A. Petrographic Identification of Reactive Minerals in Domestic Aggregates and Their Classification According to RILEM and ASTM Recommendations. *Roads Bridges-Drog. I Mosty* **2017**, *16*, 223–239. [CrossRef]
11. Bourdot, A.; Thiéry, V.; Bulteel, D.; Cuchet, S.; Hammerschlag, J.G. Alkali-Reactivity of a Swiss Siliceous Limestone Caused by Finely Dispersed Quartz. *Cem. Concr. Compos.* **2018**, *91*, 97–107. [CrossRef]
12. Custódio, J.; Costa, D.; Ribeiro, A.B.; Silva, A.S. Assessment of Potential Alkali-Silica Reactivity of Aggregates for Concrete. *Procedia Struct. Integr.* **2021**, *37*, 590–597. [CrossRef]
13. *NO-17-A204*; Nawierzchnie Lotniskowe-Nawierzchnie z Betonu Cementowego-Wymagania i Metody Badań. Ministerstwo Obrony Narodowej: Warsaw, Poland, 2015.
14. Fanijo, E.O.; Kolawole, J.T.; Almakrab, A. Alkali-Silica Reaction (ASR) in Concrete Structures: Mechanisms, Effects and Evaluation Test Methods Adopted in the United States. *Case Stud. Constr. Mater.* **2021**, *15*, e00563. [CrossRef]
15. Saha, A.K.; Khan, M.N.N.; Sarker, P.K.; Shaikh, F.A.; Pramanik, A. The ASR Mechanism of Reactive Aggregates in Concrete and Its Mitigation by Fly Ash: A Critical Review. *Constr. Build. Mater.* **2018**, *171*, 743–758. [CrossRef]
16. Ramos, V.; Fernandes, I.; Santos Silva, A.; Soares, D.; Fournier, B.; Leal, S.; Noronha, F. Assessment of the Potential Reactivity of Granitic Rocks-Petrography and Expansion Tests. *Cem. Concr. Res.* **2016**, *86*, 63–77. [CrossRef]
17. Jóźwiak-Niedźwiedzka, D.; Antolik, A.; Dziedzic, K.; Glinicki, M.A.; Gibas, K. Resistance of Selected Aggregates from Igneous Rocks to Alkali-Silica Reaction: Verification. *Roads Bridges-Drog. I Mosty* **2019**, *18*, 67–83. [CrossRef]
18. Fernandes, I.; dos Anjos Ribeiro, M.; Broekmans, M.A.T.M. *Petrographic Atlas: Characterisation of Aggregates Regarding Potential Reactivity to Alkalis*; Springer: Dordrecht, The Netherlands, 2016.
19. Fernandes, I.; Noronha, F.; Teles, M. Microscopic Analysis of Alkali-Aggregate Reaction Products in a 50-Year-Old Concrete. *Mater. Charact.* **2004**, *53*, 295–306. [CrossRef]

20. Lahdensivu, J.; Köliö, A.; Husaini, D. Alkali-Silica Reaction in Southern-Finland's Bridges. *Case Stud. Constr. Mater.* **2018**, *8*, 469–475. [CrossRef]
21. Shayan, A. Alkali Reactivity of Deformed Granitic Rocks: A Case Study. *Cem. Concr. Res.* **1993**, *23*, 1229–1236. [CrossRef]
22. Pacheco Torgal, F.; Castro-Gomes, J.P. Influence of Physical and Geometrical Properties of Granite and Limestone Aggregates on the Durability of a C20/25 Strength Class Concrete. *Constr. Build. Mater.* **2006**, *20*, 1079–1088. [CrossRef]
23. Antolik, A.; Jóźwiak-Niedźwiedzka, D. Assessment of the Alkali-Silica Reactivity Potential in Granitic Rocks. *Constr. Build. Mater.* **2021**, *295*, 123690. [CrossRef]
24. Pourebrahimi, M.; Shahhosseini, V.; Ramezanianpour, A.A. Innovative Sieve Simulation and Microstructure Image Analysis Techniques for Estimation of Aggregate Size Distribution in Hardened Concrete. *Constr. Build. Mater.* **2023**, *384*, 131456. [CrossRef]
25. Miguel Solak, A.; José Tenza-Abril, A.; Eugenia García-Vera, V. Adopting an Image Analysis Method to Study the Influence of Segregation on the Compressive Strength of Lightweight Aggregate Concretes. *Constr. Build. Mater.* **2022**, *323*, 126594. [CrossRef]
26. Kamani, M.; Ajalloeian, R. Investigation of the Changes in Aggregate Morphology during Different Aggregate Abrasion/Degradation Tests Using Image Analysis. *Constr. Build. Mater.* **2022**, *314*, 125614. [CrossRef]
27. Nguyen, A.; Gharehbaghi, V.; Thach, N.; Sterling, L.; Inayat, U.; Crawford, S. ASR Crack Identification in Bridges Using Deep Learning and Texture Analysis. *Structures* **2023**, *50*, 494–507. [CrossRef]
28. Shakoorioskooie, M.; Griffa, M.; Leemann, A.; Zboray, R.; Lura, P. Quantitative Analysis of the Evolution of ASR Products and Crack Networks in the Context of the Concrete Mesostructure. *Cem. Concr. Res.* **2022**, *162*, 106992. [CrossRef]
29. Bourdot, A.; Thiéry, V.; Bulteel, D.; Hammerschlag, J. Effect of Burnt Oil Shale on ASR Expansions: A Petrographic Study of Concretes Based on Reactive Aggregates. *Constr. Build. Mater.* **2016**, *112*, 556–569. [CrossRef]
30. Castro, N.; Wigum, B.J. Assessment of the Potential Alkali-Reactivity of Aggregates for Concrete by Image Analysis Petrography. *Cem. Concr. Res.* **2012**, *42*, 1635–1644. [CrossRef]
31. *PN-EN-1097-6:2002*; Tests for Mechanical and Physical Properties of Aggregates-Part 6: Determination of Particle Density and Water Absorption. Polish Committee for Standardization: Warsaw, Poland, 2002.
32. Owsiak, Z. *Korozja Wewnętrzna Betonu*; Wydawnictwo Politechniki Świętokrzyskiej: Kielce, Poland, 2015.
33. Ratnam, M. *Monograph on Alkali Aggregate Reaction*; Central Soil & Materials Research Station: New Delhi, India, 2008.
34. *ASTM C 295*; American Society for Testing and Materials, Standard Guide for Petrographic Examination of Aggregates for Concrete. ASTM International: West Conshohocken, PA, USA, 2019.
35. *ASTM C 1260*; American Society for Testing and Materials, Standard Test Method for Potential Alkali Reactivity of Aggregates (Mortar-Bar Method). In Annual Book of ASTM Standards; ASTM International: West Conshohocken, PA, USA, 2014.
36. *ASTM C 1293*; American Society for Testing and Materials, Standard Test Method for Determination of Length Change of Concrete Due to Alkali-Silica Reaction. In Annual Book of ASTM Standards; ASTM International: West Conshohocken, PA, USA, 2014.
37. Alaejos, P.; Lanza, V. Influence of Equivalent Reactive Quartz Content on Expansion Due to Alkali Silica Reaction. *Cem. Concr. Res.* **2012**, *42*, 99–104. [CrossRef]
38. Ng, T.F.; Yeap, E.B. Potential Alkali-Silica Reaction in Aggregate of Deformed Granite. *Bull. Geol. Soc. Malaysia* **2007**, *53*, 81–88. [CrossRef]
39. Ramos, V.; Fernandes, I.; Santos Silva, A. Petrographic Characterization of Granitic Aggregates. Comparison with the Results from Laboratory Tests. In Proceedings of the 13th Euroseminar on Microscopy Applied to Building Materials, Ljubljana, Slovenia, 14–18 June 2011.
40. Gibergues, A.C.; Cyr, M. Interpretation of Expansion Curves of Concrete Subjected to Accelerated Alkali–Aggregate Reaction (AAR) Tests. *Cem. Concr. Res.* **2002**, *32*, 691–700. [CrossRef]
41. Multon, S.; Sellier, A. Multi-Scale Analysis of Alkali-Silica Reaction (ASR): Impact of Alkali Leaching on Scale Effects Affecting Expansion Tests. *Cem. Concr. Res.* **2016**, *81*, 122–133. [CrossRef]